Nonequilibrium theory of polymer stretching based on the master equation

Felix Hanke and Hans Jürgen Kreuzer*
Department of Physics and Atmospheric Science, Dalhousie University, Halifax, NS, Canada B3H 3J5
(Received 13 April 2005; published 15 September 2005)

We present a model for fast polymer-stretching experiments. We use the master equation and argue that the end-to-end extension of a polymer molecule can be used as a stochastic variable after appropriate coarse graining. The main effect of increasing pulling speed or force loading rate is a marked hysteresis in the force-extension curve as well as an overall shift of the curve to higher forces when compared to the equilibrium curve. This can be understood in terms of the moments of the transition probability in the master equation. An analysis of the fluctuations and relaxation times is also given in the framework of our theory.

DOI: 10.1103/PhysRevE.72.031805 PACS number(s): 36.20.Ey, 87.15.Aa, 87.15.He

I. INTRODUCTION

A microscopic understanding of the mechanical properties of individual natural or synthetic polymer strands is required to model and predict their function in biological or technical processes, e.g., DNA replication, muscle contraction, or the rheological properties of polymers. Experimentally, single-molecule force spectroscopy with the atomic force microscope or with optical tweezers offers a versatile and powerful experimental tool to measure the extension of a single molecule as a function of applied force in different environments. The method allows one to observe the binding forces between different receptor-ligand systems [1,2] and the unfolding of protein domains [3,4], or to measure the elastic properties of individual macromolecules [5,6]. Likewise, the scanning force microscope, optical tweezers, and near-field magnetic tweezers have been used to measure the elastic response of chromosomes [7], to study formation of DNA loops by an enzyme [8], and to investigate DNA-binding molecular motors (RNA polymerase, DNA polymerase, etc.) [9], to reveal the dynamics of these molecules during translocation, as well as the effect of external force loads on their performance.

The ultimate aim of polymer science must be the explanation of the macroscopic properties of a long repetitive chain molecule in terms of the structural properties of its subunits. To proceed from the microscopic details of the quantum chemistry of these subunits to a comprehensive description of the long chain a series of well-defined approximations must be invoked that at any stage can be subjected to rigorous scrutiny. Such a program of simplifications has been in place in polymer science for many years [10], but only recently has it become practical to implement this procedure from first principles [11–13].

Macroscopic properties of immediate interest are the force-extension curve and the corresponding fluctuations of force and length of the polymer molecule. To ensure that a measurement of the force-extension relation of a polymer molecule yields the equilibrium equation of state the rate of change of the external force must be slow on the time scale of the internal relaxation of the polymer chain, which is readily checked by a sufficient variation of this rate. If the rate of increase of the external force is such that equilibrium cannot be maintained internally, nonequilibrium effects are accessed which can be used to study the kinetics and, ultimately, the dynamics of the polymer chain. As long as one stays close to equilibrium relaxation effects can be studied. These same dynamics will then also manifest themselves far from equilibrium in the form of hysteresis and nonlinearities.

A simple approach to the dynamics of polymer chains is given by the Rouse model [14,15], in which one derives a diffusion equation for the molecular motion to model the dynamics in terms of separate relaxation modes, e.g., of a linear chain of coupled harmonic oscillators. This model is appealingly simple, but it is incapable of taking into account the hydrodynamic interactions between monomers. A first solution to this problem is provided by calculating hydrodynamic corrections to the Rouse modes within the framework of the Zimm model [15]. Monte Carlo methods and molecular-dynamics simulations provide another approach to the problem [16–18].

On the experimental side, the dynamics of polymer molecules have received a lot of attention in recent years [19]. DNA molecules in particular are long enough to be observed under flow stress via fluorescent labels [20,21]. Quake and co-workers have developed a way of manipulating single DNA molecules with pairs of optical tweezers [22,23]. These experiments provide a good way to study the relaxation dynamics of biopolymers under external forces. The process of molecular relaxation is an important issue in this work, because it is one of the few ways to access molecular relaxation times [23]. The latter are important in the interpretation of virtually all polymer experiments.

There are several different approaches to measure the mechanical properties of polymers in an atomic force microscope (AFM) experiment. One is to control the spatial position and velocity of the cantilever, which suggests doing the analysis in the canonical ensemble for the equilibrium aspects. Alternatively, it is possible to control the force f and the force loading rate df/dt by implementing an additional feedback algorithm into the AFM control, which adjusts the position in such a way that only the force is controlled. Equilibrium situations of this type should be analyzed using the Gibbs ensemble. A third possibility is to use the same control

*Electronic address: h.j.kreuzer@dal.ca

to implement a force step, where f starts from a low value and is suddenly increased to some high value. All of these experiments have been done and have been shown to lead to spectacular differences, for example when looking at the unfolding of single titin domains [3]. The equilibrium theory of polymer stretching in the Gibbs and Helmholtz ensembles has been worked out by Kreuzer *et al.* [24,25].

A first-principles theory of nonequilibrium processes in polymer science would invariably have to start from the molecular energy landscape. Using the assumption that molecular stretching can be modeled as a Markov process, one can then derive a master equation. This approach has been pursued for short proteins and molecular clusters [26–28]. The energy landscape in those studies is obtained from quantum chemical calculations. Following the work of Jarzynski [29,30] it has recently become possible to measure the molecular free-energy surface directly by averaging over finite sets of nonequilibrium data [31].

In this paper we will use a different approach to study the nonequilibrium dynamics of polymers. We will model conformational conversion in the stretching of a polymer as a Markov process. This presupposes that the dynamical time scale of conversion itself is fast compared with the macroscopic kinetics of the stretching process. We will show that the model can be simplified further by taking the molecular length itself as the stochastic variable. In the resulting master equation we will argue phenomenologically for a simple form of the transition probabilities that reproduces experimental equilibrium relaxation times. Because the transition rates in the master equation must satisfy detailed balance they will contain information about the equilibrium properties of the chain. For the calculation of the latter we will use two simple models, namely, the freely jointed chain (FJC) and the freely rotating chain (FRC) models, although the generalization to more detailed polymer models is straightforward, albeit numerically more involved.

By using only the molecular length as our stochastic variable, we neglect some of the enthalpic effects observed for highly stretched and overstretched polymers. These effects have received a lot of attention in the recent literature [3,4,13,32,33] and can generally be explained with a two-state model that contains one type of short and long conformer. In this work, we will have a detailed look at the entropic regime and show some of the nonequilibrium effects one should expect to see there. We use the transfer-matrix or Green-function methods [34–36] to obtain the equilibrium properties of these models. Our theory is presented explicitly in both the Gibbs and Helmholtz regimes. This will enable us to describe realistically the experimental situations of (i) constant force loading and (ii) constant velocity of the AFM cantilevers. The situations of instant stretching and release could in principle also be treated with our theory. However, this has already been done by several groups using scaling arguments for flexible and semiflexible chains [37–41]. A detailed comparison between the two approaches will be given elsewhere.

The paper is organized as follows: in the next section we derive the specific form of the transition rates in the master equation and briefly comment on the numerical solution of the latter. We present a derivation of the macroscopic equations of motion that couple the time dependence of the average length of the polymer to the nonequilibrium evolution of the fluctuations. We then describe how to calculate the relaxation times and compare these to measured values for DNA molecules. This will enable us to estimate force loading rates and pulling velocities required to observe nonequilibrium effects. A discussion of the resulting force-extension curves as well as the fluctuations is given in Sec. III. An outline of a noncoarse-grained theory is given in the Appendix.

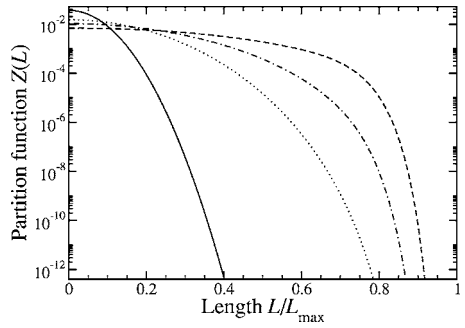

FIG. 1. The partition functions $Z(L)$ for four representative chains with $N=100$ monomers are shown on a log scale: FJC (solid line) and FRC with bond angles $\gamma=30°,45°,60°$ (dashed, dot-dashed, and dotted lines, respectively). Notice the almost Gaussian dependence of the FJC partition function.

II. THEORY

A. Equilibrium polymer properties

In order to discuss nonequilibrium polymer stretching, we first have to outline our approach to the equilibrium physics. As input for the theory in this paper, we will require the canonical partition function $Z(\mathbf{L},N,T)$, which depends on the length $\mathbf{L}$, the number of monomers N, and the temperature T. This can be calculated exactly from the transfer-matrix method developed by our group [34–36]. We will use the freely jointed chain (FJC) and freely rotating chain (FRC) models, which are good approximations for flexible and semiflexible polymers, respectively.

We would like to work in the large N limit, which means that the number of monomers must be much larger than the characteristic ratio: $N \gg C_N$. This ensures that the molecule consists of many Kuhn lengths a, so that there are no directional correlations between the two ends. The FRC characteristic ratio is given by [10]

$$C_{FRC,N} = \frac{1+\cos\gamma}{1-\cos\gamma} - \frac{2\cos\gamma}{N}\frac{1-\cos^N\gamma}{(1-\cos\gamma)^2} \tag{1}$$

while for the freely jointed chain we have $C_{\mathrm{FJC}}=1$. The characteristic ratio for $\gamma=30°$, appropriate for n-alkanes, and $N=100$ is about 13.

Figure 1 shows the partition functions $Z(N,L,T)$ for some representative chains. For the FJC, our calculations can go up to $N=150$ while $N=100$ is the limit for the FRC. This means that our FRC modeling has to be restricted to the bond angle $\gamma=60°$.

B. Master equation

1. Gibbs regime

Our study of nonequilibrium effects treats the stretching behavior of single polymer molecules as a Markov process that is represented with a master equation. If we take the index enumerating the conformers as the stochastic variable then the Markov process is defined by a function $P_i(\mathbf{f},t)$ that gives the probability that under a force $\mathbf{f}$ the ith conformer (of end-to-end length $\mathbf{L}_i$) is realized at time t. We then need as many equations of motion as there are conformers for the particular polymer. Such an approach is only feasible for "short" polymers and will be outlined in some detail in the Appendix. Here, we present a more coarse-grained approach in which we treat the end-to-end length itself as the stochastic variable.

In this approach, the force can be controlled externally; in equilibrium this corresponds to using the Gibbs ensemble (see Ref. [24] for a detailed discussion). We will refer to this mode as the Gibbs regime away from equilibrium.

We now introduce a function $P(\mathbf{L},\mathbf{f},t)$ that gives the probability that at time t the end-to-end length $\mathbf{L}$ is realized under a force $\mathbf{f}$. Its value in equilibrium is given by

$$P_{\mathrm{eq}}(\mathbf{L},\mathbf{f}) = \frac{Z(N,\mathbf{L},T)\exp(\beta\mathbf{f}\cdot\mathbf{L})}{\exp[-\beta g(T,\mathbf{f})]}. \tag{2}$$

$g(T,\mathbf{f})$ is the free energy in the Gibbs ensemble. Away from equilibrium we postulate a master equation

$$\frac{d}{dt}P(\mathbf{L},\mathbf{f},t) = \frac{1}{b^3}\int d^3L'[W(\mathbf{L},\mathbf{L}';\mathbf{f})P(\mathbf{L}',\mathbf{f},t) - W(\mathbf{L}',\mathbf{L};\mathbf{f})P(\mathbf{L},\mathbf{f},t)]. \tag{3}$$

The transition element $W(\mathbf{L}',\mathbf{L};\mathbf{f})$ gives the probability per unit time that the length of the polymer changes from $\mathbf{L}$ to $\mathbf{L}'$ under a force $\mathbf{f}$; the monomer length b being required for normalization purposes. These transition rates can in principle be calculated from the microscopic dynamics of the coupled polymer-solute system; this will be done elsewhere. Here we follow a phenomenological approach and postulate their form based on simple ideas. We argue that a small change in the force will result in, at most, a small length change over a time interval dt and write

$$W(\mathbf{L}',\mathbf{L};\mathbf{f}) \sim w_0 \exp\left[-\frac{\beta\Delta}{b^2}(\mathbf{L}'-\mathbf{L})^2\right]. \tag{4}$$

The parameter Δ controls the width of effective transitions. The prefactor

$$w_0 = \nu\exp(-Q/k_{\mathrm{B}}T) \tag{5}$$

consists of an attempt frequency ν and an energy barrier Q between two conformers. This will be discussed in detail at the end of this section. The quantity $\beta\Delta/b^2$ is typically of the order of a few inverse b^2 so that the Gaussian dependence of the transition probability W on $|\mathbf{L}'-\mathbf{L}|$ makes sure that the end of the molecule has to remain close to the starting point of a given jump. This also justifies ignoring any further dependence on $|\mathbf{L}'-\mathbf{L}|$ in Q. For longer distances, several transitions should be required.

We still need to ensure that detailed balance is satisfied for the master equation (3). Thermodynamic equilibrium not only requires that $dP/dt=0$, but that all the terms on the right-hand side of Eq. (3) vanish individually, i.e.,

$$W(\mathbf{L},\mathbf{L}';\mathbf{f})P_{\mathrm{eq}}(\mathbf{L}',\mathbf{f}) - W(\mathbf{L}',\mathbf{L};\mathbf{f})P_{\mathrm{eq}}(\mathbf{L},\mathbf{f}) = 0, \tag{6}$$

or

$$W(\mathbf{L},\mathbf{L}';\mathbf{f}) = W(\mathbf{L}',\mathbf{L};\mathbf{f})\frac{P_{\mathrm{eq}}(\mathbf{L},\mathbf{f})}{P_{\mathrm{eq}}(\mathbf{L}',\mathbf{f})} = w_0\exp\left[\beta\mathbf{f}\cdot(\mathbf{L}-\mathbf{L}') - \frac{\beta\Delta}{b^2}(\mathbf{L}'-\mathbf{L})^2\right] \times\frac{Z(N,\mathbf{L},T)}{Z(N,\mathbf{L}',T)}.$$

To ensure that the transitions $\mathbf{L}\to\mathbf{L}'$ and $\mathbf{L}'\to\mathbf{L}$ are symmetric we choose a form

$$W(\mathbf{L}',\mathbf{L};\mathbf{f}) = w_0\exp\left[\frac{\beta}{2}\mathbf{f}\cdot(\mathbf{L}'-\mathbf{L}) - \frac{\beta\Delta}{b^2}(\mathbf{L}'-\mathbf{L})^2\right] \times\sqrt{\frac{Z(L',N,T)}{Z(L,N,T)}}. \tag{7}$$

The nonequilibrium force-extension relation is given by

$$\bar{\mathbf{L}}(\mathbf{f},t) = \frac{1}{b^3}\int d^3L\ \mathbf{L}P(\mathbf{L},\mathbf{f},t) \tag{8}$$

and its equation of motion is obtained from Eq. (3),

$$\frac{d\bar{\mathbf{L}}}{dt} = \langle\alpha_1(\mathbf{L})\rangle. \tag{9}$$

We define the mean-square fluctuations of the molecular end-to-end distance as a second rank tensor,

$$\langle\overleftrightarrow{\sigma^2}\rangle = \langle\mathbf{LL}\rangle - \langle\mathbf{L}\rangle\langle\mathbf{L}\rangle. \tag{10}$$

In a coordinate system where the force points along the z axis, this tensor is diagonal. In this case, the equation of motion for an element is

$$\frac{d\langle\sigma_{ii}^2\rangle}{dt} = \langle\alpha_{2ii}\rangle + 2\langle L_i\alpha_{1i}\rangle - 2\langle L_i\rangle\langle\alpha_{1i}\rangle. \tag{11}$$

For Eqs. (9) and (11) we have defined the nth moment of the transition probabilities,

$$\vec{\alpha}_n(\mathbf{L},\mathbf{f}) = \frac{1}{b^3}\int d^3L'(\mathbf{L}'-\mathbf{L})^n W(\mathbf{L}',\mathbf{L};\mathbf{f}), \tag{12}$$

as a tensor of rank n.

To solve the master equation one discretizes the space accessible to a given molecule into a manageable number of points so that the master equation (3) becomes a set of coupled differential equations, one per mesh point. Since this would lead to a rather large and intractable system in three dimensions, we will present numerical results only for the

polymer distribution along the force axis. This reduces the problem to one dimension and the transition probabilities have the form

$$W(L',L;f) = w_0 \exp\left[\beta\frac{f}{2}(L'-L) - \frac{\beta\Delta}{b^2}(L'-L)^2\right] \times \sqrt{\frac{Z(N,L',T)}{Z(N,L,T)}}. \quad (13)$$

This corresponds to the approximation that the additional two integrations in Eq. (3) have roughly the same effect for all times. We show in Sec. II D that this approximation corresponds to the limit of small length fluctuations $\sigma_{zz}^2 \ll L_{\max}^2$.

We now discuss the origin and meaning of the attempt frequency ν in the prefactor (5). The internal excitation modes that trigger the length changes are sound waves that travel along the backbone of the polymer chain. For the longest wave spanning the length of the molecule we can write $\nu = c_s/L_{\max}$. As an example, these modes are calculated in the Rouse model by assuming that the molecule is a chain of coupled harmonic oscillators. To get more realistic estimates we have used the vibrational spectrum previously calculated with density functional theory for short chains of (methoxy-terminated) ethylene glycol monomers, EG (O-CH_2-CH_2-) [42]. For $(EG)_3$ the frequencies of longitudinal vibrations along the backbone for the helical and planar conformers are 82 and 640 cm^{-1}, respectively, with a wavelength of 10.5 Å (the contour length between the outermost O atoms). For helical $(EG)_4$ this frequency is 72 cm^{-1}, not quite down by a factor of 3/4 from the $(EG)_3$ value because of the presence of the two end groups. Likewise, for transverse vibrations we find frequencies in the range from 18 to 30 wave numbers for both conformers. Attaching several water molecules to $(EG)_3$ in order to mimic the presence of the solvent, we find that the longitudinal frequencies increase by 15–20 %.

For $(EG)_3$, we get for the speed of sound, $c_s = \nu\lambda$, about 2000 m/s and 16 000 m/s for the helical and all-trans conformers, respectively. The reason why the speed, and thus the force constant, is so much larger for the all-trans conformer is the fact that for the helical conformer the vibration involves the deformation of the dihedral angle whereas for the all-trans conformer it is the harder deformation of the C-C and C-O bond angles. Similarly we get for a short alkane chain $c_s \simeq 4500$ m/s. This leads us to identify the attempt frequency as $\nu = c_s/L_m$. The same first principle calculations for $(EG)_3$ also produced the energy landscape, i.e., potential energy curves, depicted in Fig. 2. It shows explicitly how much the force constants differ between different conformers. In addition we get an estimate of the activation energies, Q in Eq. (5), for conformational conversion, namely, up to 0.3 eV, particularly for the solvated polymer. One can also identify a very weak dependence on the length L. Needless to say that these energy landscapes include hydrodynamic effects.

So far we have only considered longitudinal sound waves along the polymer backbone as contributing in the stretching of the molecule. However, relaxation perpendicular to the direction of the force is also of importance and can be measured. This is triggered by transverse sound waves which can be accounted for by writing

$$w_0 = \gamma(\mathbf{c}\cdot\hat{\mathbf{f}})\exp[-\beta Q]/L_{\max}, \quad (14)$$

where $\mathbf{c} = (c_\parallel, c_\perp, c_\perp)$ and $\hat{\mathbf{f}}$ is a unit vector in the direction of the force. For completeness, we have also included an accommodation coefficient γ to account for the probability that not all attempts lead to a length change. It also incorporates hydrodynamic effects; this will be elaborated on in future work.

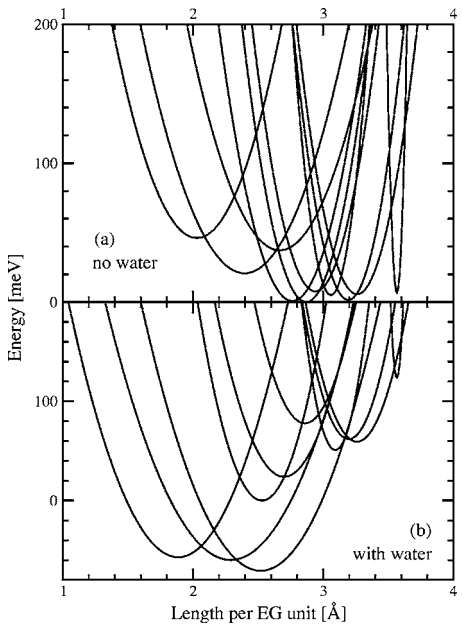

FIG. 2. The calculated energy landscape for the 10 energetically different conformers of $(EG)_3$ in vacuum and in water. These conformers are indexed by the state of the C-C bond, which can be either gauche-plus (g^+), gauche-minus (g^-), or trans (t). From left to right in plot (a) the minima belong to the conformers (g^+g^-t), $(g^+g^+g^-)$, (g^+g^-t), (g^+g^+t), $(g^+g^+g^+)$, (g^+tg^+), (g^+tg^-), (tg^+t), (ttg^+), and (ttt). When dissolved in water, the order of the minima is the same but for $(g^+g^+g^+)$ and (g^+g^+t), which change their relative positions [12,42]. Most minima are within k_BT of each other at room temperature. These curves reproduce the poly(ethylene-glycol) (PEG) stretching both in vacuum and in water [43].

2. Helmholtz regime

The discussion above treats in detail the case of controlling the force on a molecule and changing it as a known function of time. However, AFM experiments are generally done by controlling the position of the cantilever D and measuring its resulting deflection, which gives the force on the molecule as well as its stretching length. Figure 3(a) shows the schematic setup of the situation.

This approach corresponds to doing the equilibrium statistical mechanics in the Helmholtz regime. In order to do this properly, we need to take into account the exact effects of the cantilever. The approach is the same as in the Gibbs

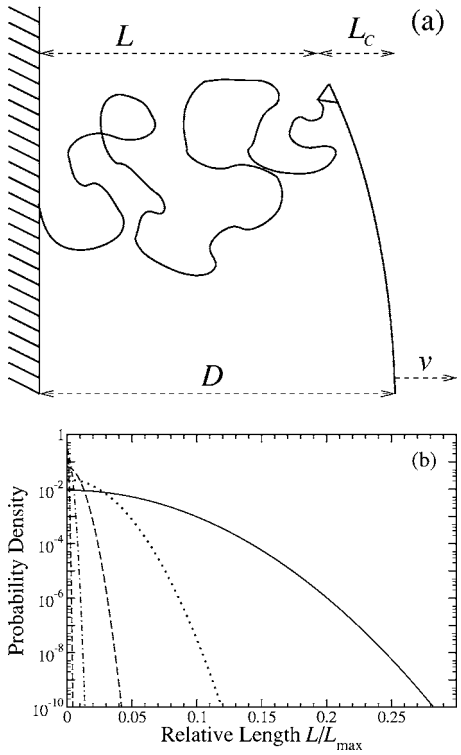

FIG. 3. (a) The basic setup of an AFM experiment, where the position D of the cantilever is controlled and the actual length of the polymer L as well as the displacement of the cantilever L_C fluctuate. (b) The end-to-end distance distribution of polymer and cantilever for $D=0$ calculated for a FJC ($N=150$) and different spring constants. The solid line has no spring attached (for comparison) and the other lines have $k_c a^2/k_B t=0.1$ (dashed), 1 (long dashed), 10 (dot-dashed), 100 (dotted line).

regime: we will use a master equation with the length as the stochastic variable. This problem will be solved entirely in one dimension, since the AFM experiments generally pull polymers vertically away from some surface. We will comment on the equivalence of the one- and three-dimensional cases in Sec. II D.

The transition probabilities still have the form $W(L',L) \sim \exp[-\beta\Delta(L'-L)^2/b^2]$, but now the equilibrium distribution for the system depends on both, L and D as [24]

$$P_{\mathrm{eq}}(L,D) = \frac{Z(L)e^{-\beta k_c (D-L)^2/2}}{\int dL\, Z(L) e^{-\beta k_c (D-L)^2/2}}. \tag{15}$$

This probability density function for different values of the cantilever spring constant k_c is shown in Fig. 3(b). For simplicity, we chose $D=0$ for those plots. One can see that the effect of a stiff cantilever is to narrow the axial end-to-end distance probability distribution of the polymer. We will discuss this point in detail below.

The introduction of a spring changes the overall transition probabilities considerably. By requiring detailed balance and with $W(L',L)$ symmetric, we find

$$W(L',L;D) = w_0 \exp\left(-\frac{\beta\Delta(L-L')^2}{b^2} + \frac{\beta k_c}{4}[(D-L)^2-(D-L')^2]\right)\sqrt{\frac{Z(L')}{Z(L)}}. \tag{16}$$

We can use this form to integrate the master equation (3) directly. The cantilevers used in the experiments by Gaub and co-workers [6,44] and other groups have spring constants around $k_c \sim 10^2$–$10^3 k_B T/b^2$. When substituting these into the equilibrium distribution (15) or the transition probabilities and hence the master equation, we find that the Gaussian dependences are almost δ functions. Taking the formal limit $k_c \to \infty$ we have, as in Ref. [24],

$$P(L,D) \sim \delta(D-L). \tag{17}$$

This is to be expected, as stiff cantilevers do not deform significantly over distances comparable to the molecular contour length. The same happens in the master equation where we find for some time-dependent cantilever position $D(t)$,

$$\frac{1}{w_0}\frac{d}{dt}P(L) = -\exp\left[\left(-\frac{\beta\Delta}{b^2}+\frac{\beta k_c}{4}\right)(D-L)^2\right]\sqrt{\frac{Z(D)}{Z(L)}}P(L) + \sqrt{\frac{4\pi}{\beta k_c}}\delta(D-L)\int dL' \times\exp\left[\left(-\frac{\beta\Delta}{b^2}+\frac{\beta k_c}{4}\right)(D-L')^2\right] \times\sqrt{\frac{Z(D)}{Z(L')}}P(L'). \tag{18}$$

For a cantilever with a finite but large spring constant, the only appreciable thermodynamic fluctuations are in the force, with almost no length fluctuations at all. The subsequent lack in spatial spread of the probability distribution makes it rather difficult to integrate the master equation numerically. One tends to be constrained to spring constants less or equal to those used experimentally, i.e., $k_c \lesssim 10^2 k_B T/b^2$.

We now address the question of equilibrium in a pulling experiment with a stiff cantilever. For finite k_c we must consider the fluctuations in both force and length. Equilibrium is attained if the system can sample all its microstates over the time scale of the experiment. In particular this means that it has time to go through all of its fluctuations. Consider what happens when we pull the molecule so fast that the equilibrium position, after a system's relaxation time, is beyond the reach of the initial fluctuations. The system could not have gotten there by a quasistatic process and must be out of equilibrium. Next we take into account that in the limit $k_c \to \infty$ the (equilibrium) length fluctuations are very small; in fact they can be described by [24]

$$\frac{\delta L}{\bar{L}} = (D/\bar{L} - 1)\frac{\delta f}{f}. \tag{19}$$

We should expect that a necessary (but not sufficient) condition for a quasistatic process is

$$(v\tau)^2 \lesssim \overline{\sigma^2}, \tag{20}$$

where τ is the relaxation time of the whole system (molecule and cantilever) and $\overline{\sigma^2}$ is the mean-square length fluctuation.

Similar to the Gibbs regime, we can define the moments of the transition probabilities in the Helmholtz regime as

$$\zeta_n(L,D) = \frac{1}{b}\int dL'(L'-L)^n W(L',L;D). \tag{21}$$

Notice that we are now dealing with one-dimensional quantities so that there is no longer a tensor character. Analogous to the analysis in the Gibbs regime, we can then write the nonequilibrium force-extension relation as

$$\frac{d\bar{L}}{dt} = \langle \zeta_1(L,D)\rangle. \tag{22}$$

The spatial fluctuations are calculated from

$$\frac{d\overline{\sigma^2}}{dt} = \langle \zeta_2(L,D)\rangle + 2\big[\langle L\zeta_1(L,D)\rangle - \langle L\rangle\langle \zeta_1(L,D)\rangle\big]. \tag{23}$$

Once we have obtained the spatial fluctuations of the molecular end, either from the complete time-dependent probability density function or the equation above, we can work out the mean-square force fluctuations $\overline{\sigma_f^2}$ via [24]

$$\overline{\sigma_f^2} = k_c^2\overline{\sigma^2}. \tag{24}$$

As we saw above the fluctuations in the length are almost negligible, but those in the force remain finite. In the pure Helmholtz regime the force is, in fact, the only quantity that can fluctuate.

C. Macroscopic equations of motion

To simplify the nonequilibrium force-extension relation we assume that the fluctuations and higher moments of the probability density are small. We can then expand the ith component of the vector $\vec{\alpha}_1$ as

$$\langle \alpha_{1i}(\mathbf{L},\mathbf{f})\rangle \simeq \alpha_{1i}(\bar{\mathbf{L}},\mathbf{f}) + \frac{1}{2}\sum_{j=1}^{3}\overline{\sigma_{jj}^2}(\mathbf{L},\mathbf{f})\frac{\partial^2}{\partial\bar{L}_j^2}\alpha_{1i}(\bar{\mathbf{L}},\mathbf{f})\Bigg|_{\mathbf{f}}, \tag{25}$$

with

$$\overline{\sigma_{jj}^2} = \overline{L_j^2} - \overline{L_j}^2. \tag{26}$$

A similar expansion is possible for the components of $\langle\vec{\vec{\alpha}}_2\rangle$. The macroscopic equations of motion for the average length (9) and the fluctuations (11) now read

$$\frac{d\overline{L_i}}{dt} = \alpha_{1i} + \frac{1}{2}\sum_{j=1}^{3}\langle\sigma_{jj}^2\rangle\frac{\partial^2\alpha_{1i}}{\partial\overline{L_j}^2}, \tag{27}$$

$$\frac{d\langle\sigma_{ii}^2\rangle}{dt} = \alpha_{2ii} + 2\langle\sigma_{ii}^2\rangle\frac{\partial\alpha_{1i}}{\partial\overline{L_j}} + \frac{1}{2}\sum_{j=1}^{3}\langle\sigma_{jj}^2\rangle\left[\frac{\partial^2\alpha_{2ii}}{\partial\overline{L_j}^2} + 2\overline{L_i}\frac{\partial^2\alpha_{1i}}{\partial\overline{L_j}^2}\right]. \tag{28}$$

All the moments and their derivatives in Eqs. (27) and (28) are evaluated at the average nonequilibrium length $\bar{\mathbf{L}}$ and the applied force $\mathbf{f}$.

We note that the first moment of the transition probability $\vec{\alpha}_1$ is zero along the equilibrium force-extension curve. This can be shown by expanding the integral (12) in terms of small $(\mathbf{f}-\mathbf{f}_{\mathrm{eq}})$. The second derivatives of its components also turn out to be zero along the equilibrium force-extension curve, so that the right hand side of (27) is identically zero for equilibrium.

Knowing the equilibrium fluctuations at zero extension, one can integrate the system (27) and (28) directly. However, this approach is only valid close to equilibrium and the computational effort in calculating the moments $\vec{\alpha}_1$ and $\overleftrightarrow{\alpha}_2$ is similar to that in the direct integration of the full master equation. We will show later that the moments presented here yield a nice graphic interpretation of nonequilibrium stretching nevertheless.

The same analysis can be done for the Helmholtz regime, by expanding the average moments $\langle\zeta_2(L,D)\rangle$ and $\langle\zeta_2(L,D)\rangle$ as defined in Eq. (21). The resulting equations of motion are of course the one-dimensional equivalents of Eqs. (27) and (28), with all the α_i replaced by ζ_i:

$$\frac{d\bar{L}}{dt} = \zeta_1 + \frac{1}{2}\overline{\sigma^2}\frac{\partial^2\zeta_1}{\partial\bar{L}^2}, \tag{29}$$

$$\frac{d\overline{\sigma^2}}{dt} = \zeta_2 + \overline{\sigma^2}\left[\frac{1}{2}\frac{\partial^2\zeta_2}{\partial\bar{L}^2} + 2\frac{\partial\zeta_1}{\partial\bar{L}}\right]. \tag{30}$$

D. Relaxation times

The relaxation time τ for a system close to equilibrium can be extracted from the Gibbs equation of motion (27) by setting $\bar{\mathbf{L}} = \mathbf{L}_{\mathrm{eq}} + \overline{\delta\mathbf{L}}$ and expanding around $\mathbf{L}_{\mathrm{eq}}$ with $\vec{\alpha}_1(\mathbf{L}_{\mathrm{eq}},\mathbf{f}) = \mathbf{0}$ so that

$$\frac{d\overline{\delta L_i}}{dt} = \frac{\partial\alpha_{1i}(\mathbf{L}_{\mathrm{eq}},\mathbf{f})}{\partial\overline{L_i}}\Bigg|_{\mathbf{f}}\overline{\delta L_i} \tag{31}$$

$$= -\frac{1}{\tau_i}\overline{\delta L_i}. \tag{32}$$

This defines two relaxation times $\tau_\parallel$ and $\tau_\perp$ in the directions parallel and perpendicular to the applied force. To evaluate the moments of the transition rates analytically we introduce $\mathbf{r} = \mathbf{L}' - \mathbf{L}$ and write

$$W(\mathbf{r},\mathbf{L};\mathbf{f}) = w_0\exp\left[-\frac{\beta\Delta}{b^2}\mathbf{r}\cdot\mathbf{r} + \frac{1}{2}\beta\mathbf{f}\cdot\mathbf{r}\right]\sqrt{\frac{Z(N,\mathbf{L}+\mathbf{r},T)}{Z(N,\mathbf{L},T)}}. \tag{33}$$

The partition function can be expanded as

$$Z(N,\mathbf{L}+\mathbf{r},T) = Z(N,\mathbf{L},T)\left[1+\mathbf{r}\cdot\frac{\nabla Z}{Z}+\frac{1}{2}\mathbf{r}\cdot\mathbf{r}\frac{\nabla^2 Z}{Z}+\cdots\right]. \tag{34}$$

Statistical mechanics dictates that the various derivatives of the partition function are related to the equilibrium force $\mathbf{f}_{\mathrm{eq}}=-k_{\mathrm{B}}T\nabla Z/(bZ)$. Using these results, we find to leading order and for a uniaxial force $\mathbf{f}=f\hat{\mathbf{z}}$,

$$W(\mathbf{r},\mathbf{L};\mathbf{f}) \simeq w_0 \exp\left[-\frac{\beta\Delta}{b^2}\mathbf{r}\cdot\mathbf{r}+\frac{1}{2}\beta(\mathbf{f}-\mathbf{f}_{\mathrm{eq}})\cdot\mathbf{r}\right] \times\left[1-\beta\frac{\mathbf{r}\cdot\mathbf{r}}{4}\frac{\partial f_{\mathrm{eq}}}{\partial L}\right]. \tag{35}$$

For long chains f_{eq} only depends on $\ell=L/L_{\max}$. Note that f_{eq} is not equal to the external force $\mathbf{f}$.

We can use the expression (35) to calculate the molecular relaxation time from the derivative of the first moment of W [see Eq. (32)]. To leading order, we get the inverse transverse and longitudinal relaxation times as

$$\frac{1}{\tau_{\parallel}} = \xi_{\parallel}\frac{\partial f}{\partial \ell}, \tag{36}$$

$$\frac{1}{\tau_{\perp}} = \xi_{\perp}\sqrt{\frac{f}{\ell}\frac{\partial f}{\partial \ell}}. \tag{37}$$

In our theory, the longitudinal and transverse friction parameters have the explicit form

$$\xi_{\parallel/\perp} = \frac{\pi^{3/2}}{4}\frac{c_{s\parallel/\perp}}{L_{\max}^2}e^{-\beta Q}\frac{b}{(\beta\Delta)^{5/2}}. \tag{38}$$

Notice that we need to differentiate between longitudinal and transverse pulse velocities due to the different nature of the two relaxation modes. Thus our master equation approach has recovered the well-known result that the relaxation time is proportional to the square of the number of monomers. We also find rightly that the longitudinal relaxation time is inversely proportional to the derivative of the force-extension relation with the overall factor of proportionality given in terms of the phenomenological parameters in the transition rates. The transverse relaxation depends on the normalized force-extension relation $f(\ell)$ as well as its derivative. Hatfield and Quake [18] postulated a different form for this dependence, but they did not take into account that $f(\ell)$ is nonlinear for large extensions. Indeed, the substitution $f(\ell)=k\ell$ into Eq. (37) recovers their result. By keeping further terms in the expansion (35) we can easily calculate the corrections needed as one studies relaxation further away from equilibrium.

We still have to discuss the conditions under which we are justified to reduce the master equation to one dimension only. We see from Eq. (35) that the effects of the transverse spread in the probability functions are mainly contained within the Gaussian dependence of the transition rates. Higher order effects are smaller by at least one additional power of $1/L_{\max}$. Thus for small fluctuations $\langle\sigma_{zz}^2\rangle \ll L_{\max}^2$, all the important phenomena happen on short length scales and higher order effects can be neglected. The difference between a full three-dimensional model and a one-dimensional equivalent is now a constant factor that stems from the integration of the master equation over the two transverse dimensions. We obtain a "one-dimensional" longitudinal relaxation time

$$\tau_{\parallel,1\mathrm{D}} \approx \frac{\pi}{\beta\Delta}\tau_{\parallel,3\mathrm{D}}. \tag{39}$$

The two formulations should be equivalent if $\tau_{\parallel,1\mathrm{D}}$ and $\tau_{\parallel,3\mathrm{D}}$ are approximately equal. This leads to the fact that Δ is about $\pi k_{\mathrm{B}}T$ or of that order.

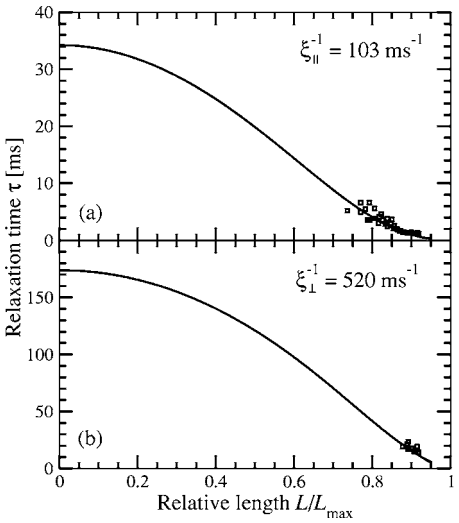

FIG. 4. The FJC fits to experimental values of the longitudinal and transverse relaxation time of λ-DNA measured by Meiners and Quake [23]. In these fits, we used the Langevin relation to determine the force-extension relation and its derivatives.

III. RESULTS

A. Relaxation times

The free parameters in our theory are w_0 and Δ. Although we gave estimates of their magnitude, we can use experimental relaxation times to determine their values for specific systems. These relaxation times have been measured for the case of λ-DNA by Meiners and Quake [23]. We need to use Eqs. (36) and (37) as well as the knowledge of the partition function (and hence the force-extension relation) in order to extract the phenomenological friction coefficients (38). Once we have obtained a values for $\zeta_{\parallel}$, it is simple to calculate the input value for w_0 as well as the size of the barrier Q. One can also make estimates about the differences between $c_{s,\parallel}$ and $c_{s,\perp}$ for a given model.

We have fitted the FJC model ($N=150$), as well as several FRC polymers with 100 monomers, to the data given in Ref. [23]. Equally good fits were obtained for the freely jointed chain and the freely rotating chain with a bond angle $\gamma=60°$. These two models will hence be used for the rest of our analysis. Figure 4 shows the fits to the DNA data obtained from the FJC model. The FRC fits are very similar and not shown here.

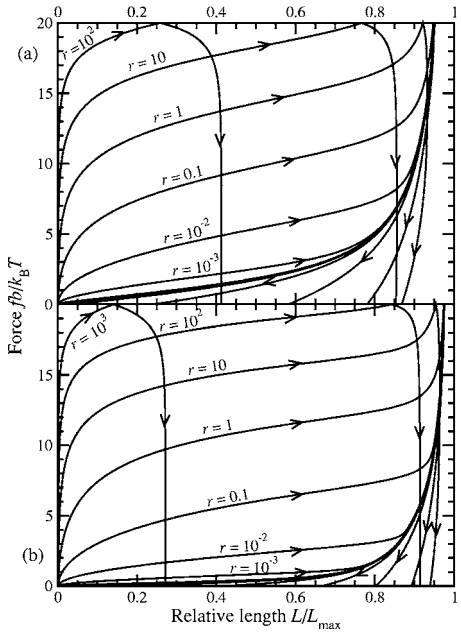

FIG. 5. The nonequilibrium force-extension relations calculated from the master equation (3) (a) for the FJC model with 150 monomers and (b) for the FRC model with 100 monomers and a bond angle of 60°. The rates r are given in dimensionless units (see text) and are used as labels for the curves. Additional (unlabeled) curves that almost coincide with the equilibrium force-extension relations are for $r=10^{-4},10^{-5}$ in plot (a) and for $r=10^{-4}$ in plot (b). The rates r are given in units of $w_0 k_B T/b$.

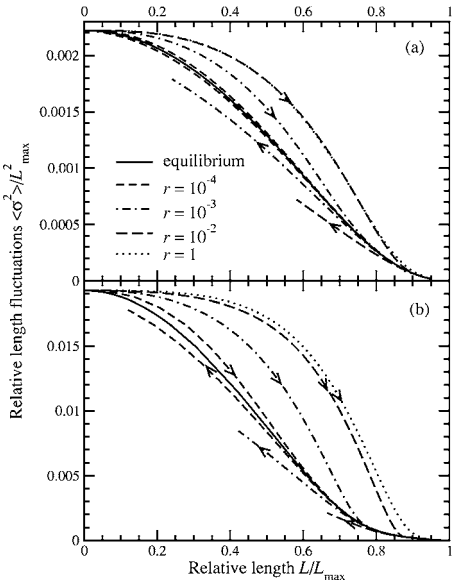

FIG. 6. The length fluctuations corresponding to the nonequilibrium force-extension curves in Fig. 5 for representative traces of both (a) the FJC model and (b) the FRC chains. Note that the $r=10^{-2}$ and $r=1$ curves in plot (a) practically overlap.

From our fitting, we obtain the parameters $\xi_{\parallel}^{-1}=103$ and 61 ms as well as $\xi_{\perp}^{-1}=522$ and 301 ms for the FJC and FRC chains, respectively. As we can see from Eq. (38) the only real difference is in the parallel and perpendicular pulse velocities, which leads to the conclusion that they have to differ by a factor of about 5. From the fitted data, we can obtain the values of w_0 to be used in the input of our theory. This will then be the basic unit of frequency for a given molecule. Along with the knowledge of the Kuhn length a (which takes the place of the monomer length b) and the thermal energy $k_B T$ we then have a complete specification of the magnitude of all relevant quantities in our calculation. Using $\beta\Delta=\pi$, the contour length $L_{\max}=16\ \mu$m, and a Kuhn length of $a=52$ nm, [18], we find $w_{0,\mathrm{FJC}}=3.8\times10^4\ \mathrm{s}^{-1}$ and $w_{0,\mathrm{FRC}}=6.3\times10^4\ \mathrm{s}^{-1}$. We can also use our order of magnitude estimate for the longitudinal pulse velocity from Sec. II B to obtain an estimate for the transition barrier, $Q\approx0.2$ eV.

Notice that these results are only for DNA, where relaxation time data is readily available. However, the knowledge of the relevant parameters in Eq. (38) or some other phenomenological estimate of the ξ will enable the analysis for other polymers as well. In fact, for a rough estimate, one can simply apply the results presented here and scale w_0 using the appropriate contour and Kuhn lengths.

B. Nonequilibrium force-extension curves in the Gibbs regime

In its discretized form the master equation (3) is a system of coupled first order differential equations. In Fig. 5 we show nonequilibrium force-extension curves for the FJC and FRC models, varying the rate r of increase of the force. Starting at zero, we increase the force linearly in time up to $fb/k_B T=20$ and then decrease back to zero at the same rate. The force loading rate r, given here in units of $w_0 k_B T/b$ is varied exponentially. For small r, we find results very close to the equilibrium force-extension relation for a given model, which can be calculated directly from the partition functions. As we increase r, the internal molecular relaxations are too slow to keep up with the increasing force, which means that the whole nonequilibrium force-extension relation is shifted upward.

When the force is decreased, the molecule remains at larger lengths than the equilibrium value for a given force f. In fact, for very fast force loading rates, the molecular length increases further despite the decreasing force. This results in an overall hysteresis that is larger for a larger rate of increase of the force and which is the obvious signature of nonequilibrium.

More information is available about the nonequilibrium relaxation curves in Fig. 5 when we plot the relative length fluctuations $\overline{\sigma^2}/L_{\max}^2=(\overline{L^2}-\bar{L}^2)/L_{\max}^2$. These are also available from the solution of the master equation. They also serve as a check for our theory, because the one-dimensional approximation to the three-dimensional theory requires $\overline{\sigma^2}/L_{\max}^2$ to be small. Figure 6 shows some representative traces of the fluctuations that correspond to the nonequilibrium force-extension curves.

First of all a note on the relative fluctuations in general. While the FJC polymer is almost purely Gaussian for small extensions, i.e., it can be modeled successfully with a classical random walk, the FRC is much stiffer which leads to larger fluctuations. This difference is observable in both the equilibrium properties as well as the hysteresis. Not surprisingly, the hysteresis in these higher moments of the molecu-

lar probability density function is much more pronounced than for the force-extension curves themselves. As indicated above, in order to be in equilibrium the fluctuations have be the same for increasing as for decreasing forces. Figure 6 shows that this is a much more restrictive criterion. In fact, when we look at the $r=10^{-4}$ trace of the FRC model, we see that the force-extension relation practically coincides with the equilibrium relation. However, the fluctuations still show rather large deviations from equilibrium. Unfortunately, our numeric method does not allow calculations below this value for r; numerical precision plays a major role when integrating the master equation with $\dot{P}(L)\approx 0$. For that type of calculation, one simply has to use the equilibrium transfer matrix approach by itself.

Next we will discuss the rates r that have been used in these calculations. The time variable used in the solution of the master equation (3) is dimensionless and has the form $\tau=w_0 t$. We have also renormalized the force $\tilde{f}=fb/k_{\mathrm{B}}T$ for the purpose of our numerical analysis. We can use the quantities derived in Sec. III A to shed some light on the meaning of those transition rates. In terms of the variable r shown on the plots in Fig. 5, the force loading rates for the two models are

$$\frac{df}{dt} = 3r \text{ nN/s for the FJC model,} \tag{40}$$

$$\frac{df}{dt} = 5r \text{ nN/s for the FRC model.} \tag{41}$$

When comparing the dimensionless force loading rates between Figs. 5(a) and 5(b), one finds that the model dynamics of the FJC are roughly 1 order of magnitude faster than those of the FRC. This can be seen in the displacement of a given curve from its equilibrium value. However, the same order of magnitude can be found in the fits to the relaxation time of both models, as shown in Eq. (40) and (41). This enables us to work out a consistent picture of DNA stretching and determines when one should be using an explicitly nonequilibrium model to understand experiments. To within an order of magnitude in r, Figs. 5 and 6 show that nonequilibrium effects become important when $r\gtrsim 10^{-3}$. Using those values and the results from the last paragraph, this corresponds to a force loading rate of about 3–5 pN/s for DNA. We see that both models predict roughly the same magnitude of the nonequilibrium effects for a given force loading rate. This adds to the confidence in our results.

An interesting observation from Fig. 5 is that the curves resemble their equilibrium counterparts above a certain critical force f_c if one shifts the force axis appropriately. This can be explained quite well on the basis of the growth of fluctuations in the nonequilibrium stretching. As pointed out above, equilibrium conditions require that the AFM cantilever moves slow enough that it samples the molecular fluctuations available to it. When doing experiments and theory in the Gibbs regime, these spatial fluctuations are quite large, because (at least in theory) the cantilever has to respond to all of the molecular motions. As soon as one upsets this fluctuation envelope, one obtains a different kind of dynamic state where the fluctuations about the mean position are skewed. In order to establish this state, one needs to pull fast and at comparatively large forces. However, once this state is established at the end of the molecule, the system is governed by roughly the same entropic properties as in the equilibrium case.

Experimentally, the force and position origins are generally chosen by looking for the point where the cantilever stops pushing on the surface. The shoulders observed in Fig. 5 look quite similar and we question this practice for high force-loading rates. While this effect is not very pronounced in the Helmholtz regime, our current results have a major impact on the interpretation of the low-force regime of the data acquired by Fernandez *et al.* [33]. These experiments were done with polysaccharide, rather than DNA, which means that the absolute force loading rates should be different. However, the soft shoulder that we calculated for the nonequilibrium curves is well visible. The force-loading rates in their experiments are between 1 and 3 nN/s, which is about the onset of the nonequilibrium regime in our theory.

C. Nonequilibrium force-extension curves in the Helmholtz regime

Next we have to discuss the Helmholtz regime, where we control the cantilever position rather than the force directly. Our calculations will proceed as follows. Initially, we increase the cantilever position D with a speed v_r (in units of bw_0), starting from zero. Once some specified maximum position is reached, we decrease it again with the same speed back to zero. If we encounter a negative force on the way, the calculation is stopped.

Unfortunately, we cannot calculate the molecular properties when a realistically stiff cantilever is used, because in this case the exponentials in the transition probability (16) become unacceptably large. We also attempted the integration of the master equation (18) in the $k_c\to\infty$ limit, but that also did not yield any useful results because the probability distribution $P(L)$ was much too sharp for our purposes. To avoid these numerical difficulties one can follow the approach outlined by Kreuzer *et al.* [12,24] and describe the effects of the cantilever entirely with an effective force $\bar{f}=k_c(D-\bar{L})$. The numerical analysis now has to be done in the Gibbs regime. This amounts to a mean-field theory and would allow us to model systems with much higher spring constants than in the exact approach. Our calculations show that fixing the force in such a manner leads to unacceptably large length fluctuations [cf. Fig. 3(b)]. The comparison between mean-field and exact calculations is not too promising.

Figure 7 shows the results obtained from the calculations with small spring constants. The natural units of velocity are given by $w_0 b$; we have these for DNA via our relaxation time fits. For the FJC model with $N=150$, we find $w_{0,\mathrm{FJC}}b=2$ mm/s, while the FRC fits result in $w_{0,\mathrm{FRC}}b=3.3$ mm/s. This gives fairly consistent results when we compare with the plots in Fig. 7: One should expect to see conformational nonequilibrium effects when DNA molecules are pulled at speeds above $v_r=0.1$ or $v\approx 200$–300 μm/s.

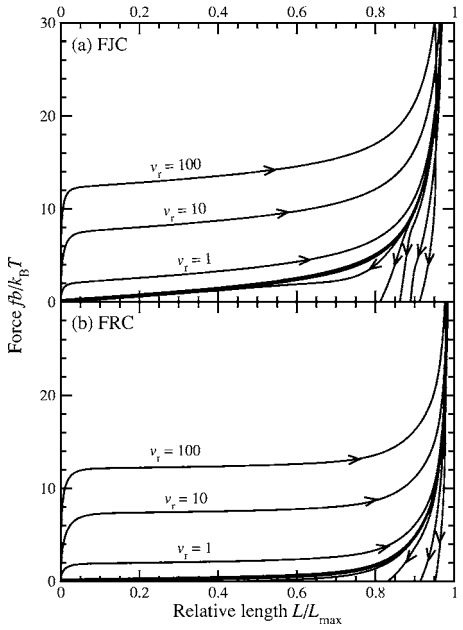

FIG. 7. The force-extension curves for $k_c = k_B T/a^2$ for the FJC chains in panel (a) and the FRC chains in panel (b). the relative dimensionless velocities $v_r = v/aw_0$ are used to label the curves.

The comparison of Fig. 7 to experiments is again not quite straightforward, because we need to estimate the time scales for each experiment separately. This is based on the values of b, L_{max}, a number for the transition barrier Q, as well as the backbone pulse velocity c_s.

For the simple polymer poly(ethylene-glycol) (PEG) these are known quite well (see Fig. 2), so we will use it as an example. In their original work, Oesterhelt *et al.* [6] used PEG with a contour length of around 400 nm and a Kuhn length of $a = 7$ Å. The barrier between a helical and a trans conformer is about $Q = 50$ meV and $c_s \approx 4500$ m/s [42,43]. In the framework of our theory, this leads to $w_0 = 1.6 \times 10^6$ s^{-1}. The onset of the nonequilibrium effects at $v_r = 0.1$ in Fig. 7 would then correspond to a pulling velocity of $v \approx 0.1$ m/s. This is well within the range of the experimental values. If one were to do experiments in the Gibbs regime, force-loading rates corresponding to $r = 10^{-3}$ are about 10 μN/s. Both of these are well above the current limits of AFM spectroscopy, which means that it is a safe assumption to treat PEG molecules as equilibrium systems, as has been done in experiments by Kudera *et al.* [44].

A rather nice demonstration of the difference between the Helmholtz and Gibbs regime is the plot of the force fluctuations (Fig. 8) corresponding to the force-extension curves presented above. These are the important fluctuations in the Helmholtz regime. Since our theory has the length as stochastic variable, we have to calculate the force fluctuations from Eq. (24). The qualitative difference to the Gibbs regime fluctuations in Fig. 6 is striking. First of all note that there is hardly any hysteresis and that the curves almost completely superimpose. The plateau for the low-extension region is due to the cantilever, which limits the overall fluctuations of the system. In this regime, the term $\exp[-\beta k_c (D-L)^2/2]$ dominates not only the equilibrium probability density (15), but

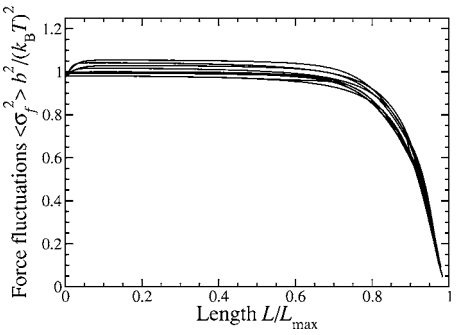

FIG. 8. The force fluctuations that correspond to all of the force-extension curves in the Helmholtz regime given in Fig. 7. There is hardly any hysteresis in these curves, because they are almost completely dominated by the properties of the cantilever, which has a spring constant of $k_c = k_B T/b^2$.

also the transition rates (16) and hence the whole master equation. In fact, one can show that the classical fluctuations of a single cantilever that is maintained at some finite extension l_c is always equal to $\langle \sigma_f^2 \rangle = k_c k_B T$ [45]. The high-extension regime of the fluctuations is controlled by the polymer, which provides the limiting factor in the system in this region.

By controlling the force in the calculation for the Gibbs regime, this effect is not present at all. The effects of the polymer on the overall fluctuations of the system only come into play once the molecule is stretched far enough such that its fluctuations become the limiting factor. From the equilibrium trace in Fig. 6 we can tell that this becomes the case around $L/L_{max} \approx 0.8$–0.9, which is indeed where the fluctuations in the Gibbs and Helmholtz regimes are the same.

We would also like to point out the slight increase of $\overline{\sigma_f^2}$ at the beginning of some curves. This corresponds to the high velocity (topmost) traces in Fig. 7. This effect naturally appears when the molecule is taken far out of equilibrium and it cannot reach all its natural equilibrium fluctuations fast enough. The fluctuation envelope lags behind and this leads to a broadening of the instantaneous molecular probability distribution $P(L,t)$.

In order to shed light on the properties of stiffer cantilevers we can solve the master equation for short times only and investigate what happens at short extensions. Figure 9 shows such results for the FJC chains only. These traces have been calculated for a velocity $v = bw_0$, because that way the probability density functions change quickly so that the numerical algorithm does not quite break down for the short times considered here. The conclusion from these calculations is quite obvious. The effect of a stiffer cantilever is a more extreme increase of the force at short length scales. This is very interesting as the cantilevers considered here are still much softer than those used for typical experiments.

To conclude this section, we want to discuss the feasibility of observing nonequilibrium effects. The force loading rates currently achieved in single protein pulling experiments are about 3 nN/s [33], which is well into the nonequilibrium range for DNA, but not necessarily for other systems. Theory suggests that pulling speeds of the order of 10 mm/s should be possible. This figure is based on a cantilever resonance

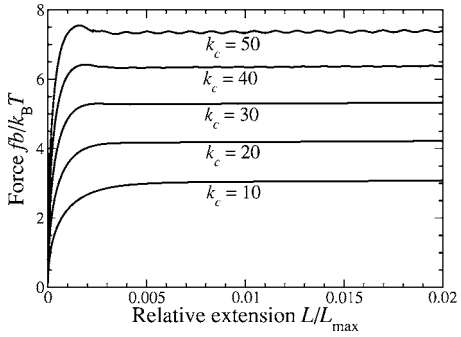

FIG. 9. The initial stages of constant velocity FJC ($N=150$) force-extension traces for stiffer cantilevers. The pulling velocity in all cases was $v_r=1$. The spring constants k_c are in the natural units of k_BT/b^2. For comparison, cantilevers that are typically used in experiments start at around $k_c \approx 100 k_BT/b^2$ at room temperature.

frequency of tens of kHz and a z range of a few microns. Anything faster would be prevented by the cantilever resonance.

D. Moments of the transition probabilities

In this section, we will discuss the moments of the transition probabilities as they occur in the macroscopic equations of motion, Eqs. (27)–(30), for the one-dimensional version of our model. In Figs. 10 and 11 we show the first and second moments, as a function of relative extension, for our FJC and FRC models.

From Eqs. (27) and (29) we see that the first moment in each regime essentially corresponds to a velocity. In fact, this velocity term is the greatest influence in the region near equilibrium where α_2 and ζ_2 are constant. The contours of the canonical moments of the transition probabilities correspond almost exactly to the nonequilibrium force-extension curves presented above, since the velocity is the controlling parameter in the corresponding calculations. In this case, the fluctuations and corrections from the gradients of ζ_2 only have a small effect. This becomes especially clear when we remember that the magnitude of the fluctuations which are controlled by the cantilever (see last section).

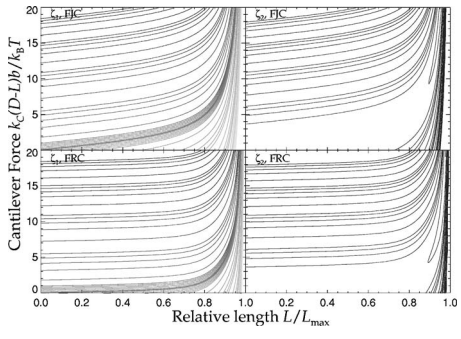

FIG. 10. Contour plots for the moments ζ_1 and ζ_2. The contours vary from values of -1000 to 1000 in levels of $\pm n \times 10^m$, where $n=\{1,2,4,6,8\}$ and $m=\{-2,-1,0,1,2\}$. The heaviest line corresponds to $\xi=1000$, while the lightest ones are for the negative ζ_1. The $\zeta=0$ contour is a little wider.

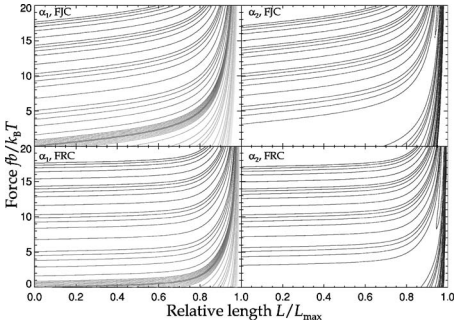

FIG. 11. Contour plots for the first two moments of the transition probabilities α_1 and α_2 in the Gibbs regime. The contours are plotted using the same scheme as in Fig. 10.

Notice that the ζ's contain the key to the rapid force increase in some of the plots in Fig. 9. The key is in the approximate relation $v \approx \zeta_1$. If we regard a pulling experiment as moving through the $f(\ell)$ plane in Fig. 10, the molecule has to reach a given ζ_1 contour as fast as possible. The fastest way to do so from the origin is to move vertically upward, that is at constant $L=0$. Once the curve has been reached, it can be traced throughout the rest of the experiment and we see exactly what has been shown in the previous section.

The situation changes for the Gibbs regime. There is no longer a one-to-one correspondence between the force-extension curves and the contours in Fig. 11, although Eqs. (27) and (28) can still be solved if we know $\alpha_1(L,f)$ and $\alpha_2(L,f)$. In the Gibbs regime we control the applied force with some force-loading rate r. At each point in time, some cantilever velocity v_c is required to maintain the required force profile. This velocity v_c roughly corresponds to the instantaneous value of α_1, while again the fluctuations and α_2 only play a minor role in this approximation.

One can now solve the approximate Eqs. (27)–(30) directly. This approach works for small extensions and very close to equilibrium. However, as one moves further away from equilibrium, the higher moments $\alpha_{i>2}$ and $\zeta_{j>2}$ become more important. In this light, it is much simpler to solve the master equation directly, although the results presented in this section provide a good intuitive understanding of the situation.

IV. DISCUSSION

In this work we have developed a theory of nonequilibrium polymer stretching in the entropic regime. We use a master equation approach with the length as our stochastic variable. We derived the transition probabilities in both the Gibbs and Helmholtz regimes and showed how they can be obtained from relaxation time measurements. We then calculated force extension curves in and out of equilibrium for two model polymers, a FJC molecule with 150 monomers and an FRC molecule with 100 monomers.

Our calculations show that one should expect nonequilibrium effects to appear when pulling at velocities of the order $0.1bw_0$ or greater. Alternatively, force loading rates of about $10^{-3}w_0k_BT/b$ will generate similar effects. For comparison with actual systems, the Kuhn length a effectively replaces

the monomer length b. We also need the transition frequency w_0, which can be estimated from Eq. (14), $w_0 \approx c_{\|} \exp(-\beta Q)/L_{\max}$. We have shown in Sec. III that w_0 can vary over several orders of magnitude, from 10^4 s^{-1} for λ-DNA to 10^6 s^{-1} for PEG.

We find that the entropic dynamics of shorter polymer chains are much too fast for current AFM experiments to register nonequilibrium effects. However, this changes with long proteins that have contour lengths of the order of many microns. In those cases, equilibrium theories can no longer be applied with force loading rates and pulling velocities of about 5 pN/s and 30 μm/s, respectively. The difference in the two cases is already manifest in the empirical dependence of the relaxation time on the monomer number, $\tau \sim N^2$. One should in fact expect that the longer molecule has much slower dynamics.

A final point has to be made on the fluctuations, particularly in the analysis of the Gibbs regime. Our whole theory is based on the fact that a cantilever can follow the molecular fluctuations on a similar time scale. This should practically cancel the effect of the cantilever itself. As shown by Kreuzer *et al.* [24], one can achieve these conditions much more easily with a very soft cantilever. Still, the question remains whether or not it is possible in practice to follow these fluctuations one by one. Once again, the relevant quantity here is the frequency w_0. One should only be able to follow the fluctuations if the cantilever position can be monitored with a frequency $w_0 \sim 10^4$–10^5 s^{-1} for λ-DNA. If this can be achieved, one should be able to do measurements on polymers in the Gibbs regime in order to verify some of the results presented here. Again, it might be easier to do this at low temperature. Notice that the force fluctuations that correspond to the stiff cantilever actually have been observed for some systems, see, for example, Ref. [46], and have been shown to yield additional interesting information about the elastic properties of polymers [47]. Current work in progress is the microscopic derivation of the transition probabilities including solvent effects. We are also looking at the derivation of the Fokker-Planck equation.

ACKNOWLEDGMENTS

We would like to thank M. Jericho for very stimulating discussions. This work was supported in part by the Office of Naval Research and the National Science and Engineering Council of Canada. F.H. would like to acknowledge financial support from the Killam Trusts.

APPENDIX: THEORY FROM THE CONFORMERS

In this appendix we briefly outline the approach to nonequilibrium phenomena in the stretching of a polymer starting from the level of probability functions for the conformers themselves. Let $P_i(T,\mathbf{L},\mathbf{f},t)$ give the probability that under a force $\mathbf{f}$ the ith conformer (of end-to-end length $\mathbf{L}$) is realized at time t. Conformers are local minima in the electronic energy surface of the polymer molecule in a space spanned by 3^{nN} coordinates of its atoms where N is the number of monomers and n is the number of atoms per monomer. This energy surface can be mapped for short polymers (invoking a number of criteria) using first principles calculations based, for instance, on density functional theory as recently demonstrated for poly(ethylene glycol). The result is a set of energy curves, $E_i(\mathbf{L})$, for the ith conformer stretched to a length $\mathbf{L}$ around its minimum at $\mathbf{L_i}$ and also all the vibrational and rotational frequencies. Likewise, transition states can be identified that lead from one conformer to another.

In equilibrium the conformer probability function is given by

$$P_i^{eq}(T,\mathbf{L},\mathbf{f}) = \frac{\exp[-\beta E_i(\mathbf{L})]\exp[\beta \mathbf{f}\cdot\mathbf{L}]}{\exp[-\beta g(T,\mathbf{f})]}. \tag{A1}$$

To study nonequilibrium effects we again assume that the stretching the molecule can be described by a homogeneous Markov process satisfying a master equation

$$\frac{d}{dt}P_i(T,\mathbf{L},\mathbf{f};t) = \sum_{j,\mathbf{L}'} [W(i,\mathbf{L};j,\mathbf{L}';\mathbf{f})P_j(T,\mathbf{L}',\mathbf{f};t) - W(j,\mathbf{L}';i,\mathbf{L};\mathbf{f})P_i(T,\mathbf{L},\mathbf{f};t)]. \tag{A2}$$

One acceptable form of the transition probabilities is given by transition state theory

$$W(j,\mathbf{L}';i,\mathbf{L};\mathbf{f}) = \frac{z_{ji}^{\#}(\mathbf{L}',\mathbf{L})}{z_i(\mathbf{L})}\exp\left(-\beta[E_{ji}(\mathbf{L}',\mathbf{L}) - E_i(\mathbf{L})] + \frac{1}{2}\beta\mathbf{f}\cdot(\mathbf{L}'-\mathbf{L})\right), \tag{A3}$$

where $z_i(\mathbf{L})$ and $z_{ji}^{\#}(\mathbf{L}',\mathbf{L})$ are the partition functions accounting for the internal vibrations and rotations of the polymer around the minimum of the ith conformer and at the transition state of energy E_{ij} to the jth conformer. Some of these numbers have been calculated for short chains, for instance n-alkanes and oligo-ethylene.

It should be obvious that all this information needed to specify the transition probabilities (A3) can at best be obtained for short chains [11,12] as done very successfully in recent years in the study of proteins [26–28].

To make the connection with the approach presented in this paper we must invoke simplifying assumptions. In particular, if the conformational conversion for a given length and conformer is fast on the time scale of stretching we can write

$$P_i(\mathbf{L},\mathbf{f};t) = \exp[-\beta E_i(\mathbf{L})]P(\mathbf{L},\mathbf{f};t) \tag{A4}$$

and the master equation simplifies to

$$\frac{d}{dt}P(\mathbf{L},\mathbf{f};t) = \sum_{\mathbf{L}'} [W(\mathbf{L};\mathbf{L}';\mathbf{f})P(\mathbf{L}',\mathbf{f};t) - W(\mathbf{L}';\mathbf{L};\mathbf{f})P(\mathbf{L},\mathbf{f};t)], \tag{A5}$$

where

$$W(\mathbf{L},\mathbf{L}';\mathbf{f}) = \frac{\sum_{i,j} W(i,\mathbf{L};j,\mathbf{L}',\mathbf{f})\exp[-\beta E_j(\mathbf{L}')]}{\sum_i \exp[-\beta E_i(\mathbf{L})]} \tag{A6}$$

is the transition probability specified phenomenologically at the beginning of this work.

[1] D. U. Lee, D. A. Kidwell, and R. J. Colton, Langmuir **10**, 354 (1994).
[2] V. T. Moy, E.-L. Florin, and H. E. Gaub, Science **266**, 257 (1994).
[3] A. F. Oberhauser, P. K. Hansma, M. Carrion-Vasquez, and J. M. Fernandez, Proc. Natl. Acad. Sci. U.S.A. **98**, 468 (2001).
[4] M. Rief, F. Oesterhelt, B. Heymann, and H. E. Gaub, Science **275**, 1295 (1997).
[5] M. Rief, M. Gautel, F. Oesterhelt, J. M. Fernandez, and H. E. Gaub, Science **276**, 1109 (1997).
[6] F. Oesterhelt, M. Rief, and H. E. Gaub, New J. Phys. **1**, 6.1 (1999).
[7] J. Yan, D. Skoko, and J. F. Marko, Phys. Rev. E **70**, 011905 (2004).
[8] J. Yan and J. F. Marko, Phys. Rev. E **68**, 011905 (2003).
[9] C. Bustamante, Y. R. Chemla, N. R. Forde, and D. Izhaky, Annu. Rev. Biochem. **73**, 705 (2004).
[10] P. J. Flory, *Statistical Mechanics of Chain Molecules* (Hanser/Gardner Publications, Inc., Cincinnati, 1988).
[11] H. J. Kreuzer, R. L. C. Wang, and M. Grunze, New J. Phys. **1**, 21.1 (1999).
[12] H. J. Kreuzer and M. Grunze, Europhys. Lett. **55**, 640 (2001).
[13] T. Hugel, M. Rief, M. Seitz, H. E. Gaub, and R. R. Netz, Phys. Rev. Lett. **94**, 048301 (2005).
[14] P.-G. de Gennes, *Scaling Concepts in Polymer Physics* (Cornell University Press, Ithaca, NY,1979).
[15] A. Y. Grosberg and A. R. Khokhlov, *Statistical Physics of Macromolecules* (AIP, New York, 1994).
[16] Y.-J. Sheng, P.-Y. Lai, and H.-K. Tsao, Phys. Rev. E **56**, 1900 (1997).
[17] P.-Y. Lai, Y.-J. Sheng, and H.-K. Tsao, Physica A **254**, 280 (1998).
[18] J. W. Hatfield and S. R. Quake, Phys. Rev. Lett. **82**, 3548 (1999).
[19] X. Zhuang and M. Rief, Curr. Opin. Struct. Biol. **13**, 88 (2003).
[20] T. T. Perkins, S. R. Quake, D. E. Smith, and S. Chu, Science **264**, 822 (1994).
[21] S. Manneville, P. Cluzel, J.-L. Viovy, D. Chatenay, and F. Caron, Europhys. Lett. **36**, 413 (1996).
[22] S. R. Quake, H. Babcock, and S. Chu, Nature (London) **388**, 151 (1997).
[23] J.-C. Meiners and S. R. Quake, Phys. Rev. Lett. **84**, 5014 (2000).
[24] H. J. Kreuzer, S. H. Payne, and L. Livadaru, Biophys. J. **80**, 2505 (2001).
[25] H. J. Kreuzer and S. H. Payne, Phys. Rev. E **63**, 021906 (2001).
[26] K. D. Ball and R. S. Berry, J. Chem. Phys. **109**, 8557 (1998).
[27] Y. Levy, J. Jortner, and O. M. Becker, J. Chem. Phys. **115**, 10533 (2001).
[28] Y. Levy, J. Jortner, and O. M. Becker, Proc. Natl. Acad. Sci. U.S.A. **98**, 2188 (2001).
[29] C. Jarzynski, Phys. Rev. Lett. **78**, 2690 (1997).
[30] C. Jarzynski, Phys. Rev. E **56**, 5018 (1997).
[31] O. Braun, A. Hanke, and U. Seifert, Phys. Rev. Lett. **93**, 158105 (2004).
[32] M. Rief, J. M. Fernandez, and H. E. Gaub, Phys. Rev. Lett. **81**, 4764 (1998).
[33] P. E. Marszalek, H. Li, A. F. Oberhauser, and J. M. Fernandez, Proc. Natl. Acad. Sci. U.S.A. **99**, 4278 (2002).
[34] L. Livadaru, Ph. D. thesis, Dalhousie University, Halifax, 2002.
[35] L. Livadaru, R. R. Netz, and H. J. Kreuzer, Macromolecules **36**, 3732 (2003).
[36] L. Livadaru and H. J. Kreuzer, New J. Phys. **5**, 95.1 (2003).
[37] F. Brochard-Wyart, Europhys. Lett. **23**, 105 (1993).
[38] F. Brochard-Wyart, H. Hervet, and P. Pincus, Europhys. Lett. **26**, 511 (1994).
[39] F. Brochard-Wyart, Europhys. Lett. **30**, 387 (1995).
[40] U. Seifert, W. Wintz, and P. Nelson, Phys. Rev. Lett. **77**, 5389 (1996).
[41] O. Hallatschek, E. Frey, and K. Kroy, Phys. Rev. Lett. **94**, 077804 (2005).
[42] R. L. C. Wang, H. J. Kreuzer, and M. Grunze, Phys. Chem. Chem. Phys. **2**, 3613 (2000).
[43] L. Livadaru, R. R. Netz, and H. J. Kreuzer, J. Chem. Phys. **118**, 1404 (2003).
[44] M. Kudera, C. Eschbaumer, H. E. Gaub, and U. S. Schubert, Adv. Funct. Mater. **13**, 615 (2003).
[45] T. L. Hill, *Statistical Mechanics—Principles and Selected Applications* (Dover, New York, 1987).
[46] C. Friedsam, A. del Campo Bécares, U. Jonas, M. Seitz, and H. E. Gaub, New J. Phys. **6**, 9 (2004).
[47] F. Hanke, L. Livadaru, and H. J. Kreuzer, Europhys. Lett. **69**, 242 (2005).